GEOPHYSICAL RESEARCH LETTERS, VOL. 26, NO. 1, PAGES 111-114, JANUARY 1, 1999

Permeability-porosity relationship in vesicular basalts

Martin O. Saar and Michael Manga

Department of Geological Sciences, University of Oregon, Eugene, OR 97403, USA

Abstract. The permeability k and porosity ϕ of vesicular basalts are measured. The relationship between k and ϕ reflects the formation and emplacement of the basalts and can be related to the crystal and vesicle microstructure obtained by image analysis. Standard theoretical models relating k and ϕ that work well for granular materials are unsuccessful for vesicular rocks due to the fundamental difference in pore structure. Specifically, k in vesicular rocks is governed by apertures between bubbles. The difference between calculated and measured k reflects the small size of these apertures with aperture radii typically $O(10)$ times smaller than the mean bubble radii.

Introduction

Most studies of the relationship between porosity ϕ, permeability k, and microstructure have considered granular materials, from classical treatments [e.g., *Carman,* 1956] to more recent studies [e.g., *Dullien,* 1992, p. 266; *Bosl et al.,* 1998]. By contrast very little research has been done on vesicular rocks [e.g., *Klug and Cashman,* 1996], even though basalts form important aquifers in the Pacific Northwest [e.g., *Manga*, 1997] and Hawaii [e.g., *Ingebritsen and Scholl*, 1993]. While the fracture permeability probably determines effective k of aquifers composed of volcanic rocks, interfracture ϕ and k may govern transport and diffusion processes [e.g., *Sanford*, 1997].

Here we report measurements of permeability, total, and connected porosity and investigate the microstructure (shape, size, and orientation of small features such as bubbles and crystals) of vesicular basalts. We interpret measurements in terms of both dynamical processes in active lavas and theoretical k-ϕ models and find a method to estimate the mean inter-bubble aperture size.

Samples and measurements

Sample cores are drilled from unfractured blocks of minimally weathered Holocene and Pleistocene basaltic andesite flows and cinder cones in the Oregon Cascades (for exact location see *Saar* [1998]). Cores have a diameter of 7.2 cm and lengths l of 2 cm $< l <$ 23 cm, such that $l \gg$ average bubble radius. Permeability is determined using a steady-state gas permeameter. Cores with high k show a non-linear relationship between pressure gradient ∇P and flow rate Q due to inertial effects. To account for inertia, we measure several sets of ∇P and Q at steady-state conditions in order to determine true k [e.g., equation (5.11.2) in *Bear,* 1988]. We also account for gas compressibility [e.g., equation (1.1.6) in *Dullien,* 1992].

Paper number 1998GL900256.
0094-8276/99/1998GL900256$05.00

Rocks are powdered to measure the matrix density and to determine the total porosity ϕ. Connected porosity ϕ_c is determined using a gas expansion technique [*Sahimi,* 1995, p. 52]. The timescale over which ϕ_c is measured, less than about 5 minutes, is much shorter than the time required for gas to diffuse across films separating bubbles.

The microstructure of our samples is investigated by both macroscopic and microscopic analysis. First, discs representing cross-sections of the cores are prepared for high resolution scanning at 1200 dots per inch (dpi). The pores are filled with white spray paint and plaster and then polished. Second, thin sections are prepared for each core. Based on the occurrence and shape of bubbles, micropores, and crystals, the samples are divided into five categories: scoria, flow1, flow2, diktytaxitic basalt [*Chitwood*, 1994], and samples containing micropores only (Fig. 1). We determine the median cross sectional bubble area for each core by analyzing 200 to 2000 bubbles (depending on bubble size) using NIH-Image. Thin section images and quantitative results on the shapes of bubbles are presented in *Saar* [1998].

Results

Figure 2a shows k versus ϕ for the five sample types: scoria, flow1, flow2, diktytaxitic, and micropore samples. Sample types plot in distinct clusters, suggesting a dependence of k and ϕ on the microstructure. Samples containing micropores only show very small k. Micropores therefore do not contribute significantly to the high k observed in the other samples. Only scoria samples show a clear relationship between k and ϕ. k falls within the range of 10^{-14} m^2 $< k < 10^{-9}$ m^2 reported by *Freeze and Cherry,* [1979, p. 29] for vesicular basalts.

Figure 2b compares total porosity ϕ and connected porosity ϕ_c. Measurements of ϕ may be underestimated because of incomplete elimination of micropores during the powdering process used to determine matrix density. Measurements of ϕ_c are more likely to include small pores and therefore plot slightly above ϕ values, indicating that virtually all pores (bubbles) in scoria, flow1, and flow2 samples are connected.

Discussion

In order to compare samples containing different bubble sizes, we normalize k by the median cross-sectional bubble area A_c for each core. *Bosl et al.,* [1998], for example, follow a similar approach for granular materials by normalizing k by the grain diameter squared.

Percolation theory suggests a power law relationship between ϕ and k of the form [e.g., *Sahimi,* 1994]

$$k(\phi) = c(\phi - \phi_{cr})^{\mu}. \qquad (1)$$

Here, c is a constant that determines the magnitude of calculated k; ϕ_{cr} is the critical porosity (percolation threshold), the minimum ϕ at which a connected pathway through

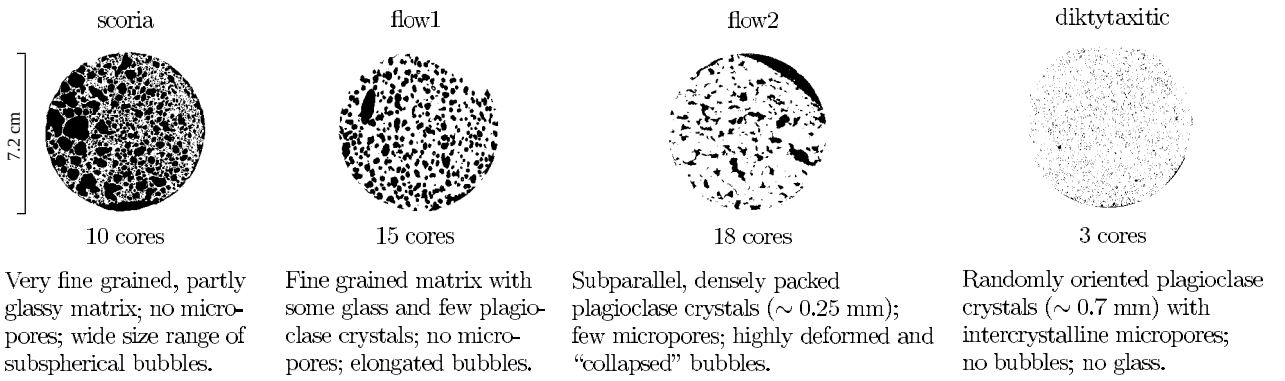

Figure 1. Scanned images (white: solid, black: bubble) and characteristics of the four main rock categories. The 3 samples containing micropores only are not included.

the sample will exist; and μ is an exponent related to the pathway geometry. For the fully penetrable sphere (FPS) model, in which the percolating objects are voids, $\mu = 2$ and $\phi_{cr} = 30\%$ [e.g., *Feng et al.,* 1987; *Sahimi,* 1994, 1995; *Mukhopadhyay and Sahimi,* 1994; *Saar,* 1998]. The FPS model might reasonably be expected to represent scoria samples which contain randomly distributed, spherical bubbles that have undergone coalescence [*Cashman et al.*, 1994].

Figure 3 shows the normalized permeability k/A_c versus ϕ along with a percolation theory curve. Percolation theory is only valid at, and slightly above, ϕ_{cr}. The constant c in equation (1) does not influence the shape of the curve and is chosen to scale the curve to k measurements on samples with subspherical bubbles and $30\% < \phi < 50\%$. Because no sample-spanning fluid pathway should exist for samples with $\phi < \phi_{cr}$, k might be expected to be zero though micropores always provide a finite k (Fig. 2a). In contrast to percolation theory predictions, we find high k at $\phi < \phi_{cr}$ and $\phi_c \approx \phi$ for all ϕ in all three rock types. This observation suggests that dynamical processes in lavas affect the vesicularity and vesicle structure and are reflected in a k-ϕ relationship that diverges from percolation theory.

One can observe a systematic increase in bubble elongation and distortion from scoria to flow1, and finally, to flow2 samples (Fig. 1). Simultaneously, the inter-bubble phase changes from a mostly glassy matrix (scoria), to a matrix containing small crystals and little glass (flow 1), and finally to a fully-crystalline, fine-grained matrix (flow 2) [*Saar*, 1998].

Scoria forms by expansion and coalescence of bubbles during decompression [*Cashman et al.*, 1994]. Rapid chilling of scoria samples during the early emplacement stage preserves the subspherical bubbles forming a bicontinuous network typical for the fully penetrable sphere (FPS) model with $\phi_{cr} < \phi < 98\%$ [e.g., *Sahimi*, 1995]. The inter-bubble phase consists mostly of glass. Since the short cooling times are likely to prevent significant inter-bubble film relaxation, preserving small aperture widths, the FPS model describes the k-ϕ relationship of scoria samples reasonably well. Flow1 samples have probably reached ϕ_{cr} as well but cooled more slowly. Bubbles probably deform due to flow, and, due to longer cooling times, apertures widen from inter-bubble film relaxation, leading to an increase in k. Larger k also allows gas to escape [e.g., *Klug and Cashman*, 1996], which in turn decreases ϕ (see Fig. 3). Flow2 samples may show a continuation of the process described for flow1 samples, ending with bubble "collapse." This extreme narrowing of the pathway does not appear to close the highly connected bicontinuous network, explaining the high pore-space connectivity of all three rock types. The result is probably a counterintuitive evolutionary trend of decreasing ϕ accompanied by increasing k/A_c away from the percolation theory curve (Fig. 3).

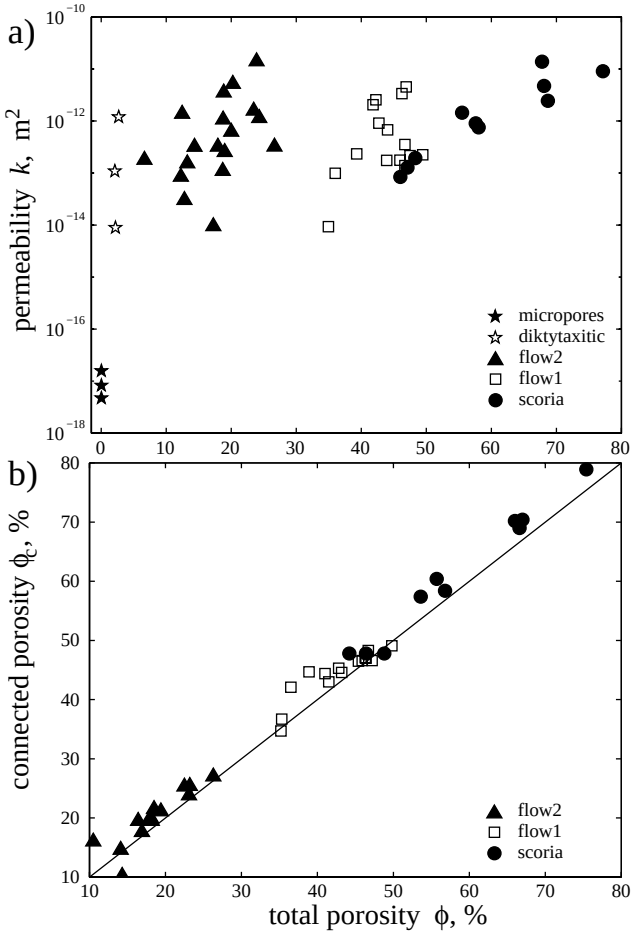

Figure 2. a) Permeability k versus total porosity ϕ for all samples ; b) connected ϕ_c versus total porosity for samples containing bubbles.

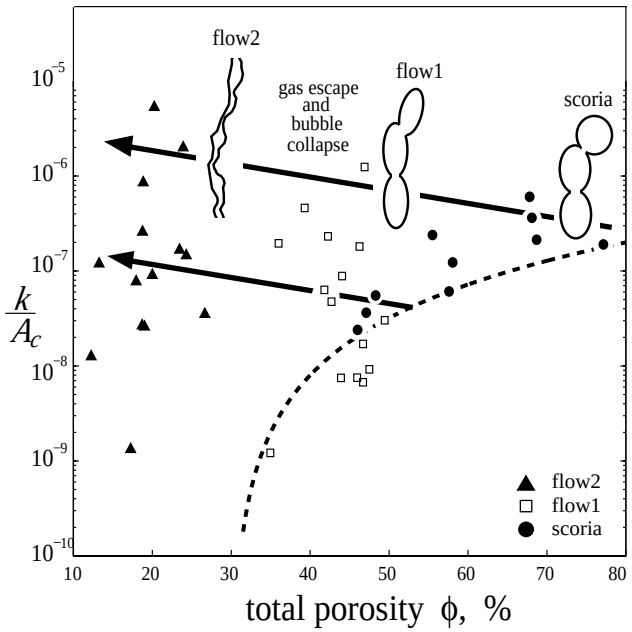

Figure 3. Permeability normalized by median cross-sectional bubble area k/A_c versus total porosity ϕ. Arrows and sketches illustrate the evolution of k/A_c due to dynamic processes. The prediction of percolation theory, equation (1), is shown with a dashed curve.

The diktytaxitic samples do not contain bubbles and are therefore not included in Figure 3.

A more quantitative understanding of the effects of vesicular microstructure can be obtained by applying theoretical k-ϕ models. The equivalent channel form [*Paterson*, 1983] of a Kozeny-Carman equation [*Carman*, 1956] is

$$k = \frac{\phi^2}{\Lambda F s^2}. \qquad (2)$$

Here s is the specific surface area, i.e., the surface area of the bubble-rock interface per unit volume; F is the formation factor, a measure of the pathway tortuosity; Λ is a constant equal to 2 for circular tubes. F is determined by Archie's law, $F = \phi^{-m}$, where $m = 1.5$ for perfect spheres, with larger m being appropriate for less spherical shapes [*Archie,* 1942; *Sen et al.,* 1981]. Here we assume $m = 2$ due to subspherical bubbles. We determine s using two-point correlation functions [*Berryman,* 1984, 1987] to analyze our scanned core images. This approach so far has been used successfully to calculate k for granular materials such as welded glass beads and Berea sandstone [e.g., *Blair et al.*, 1996]. Here we apply these ideas to vesicular basalt.

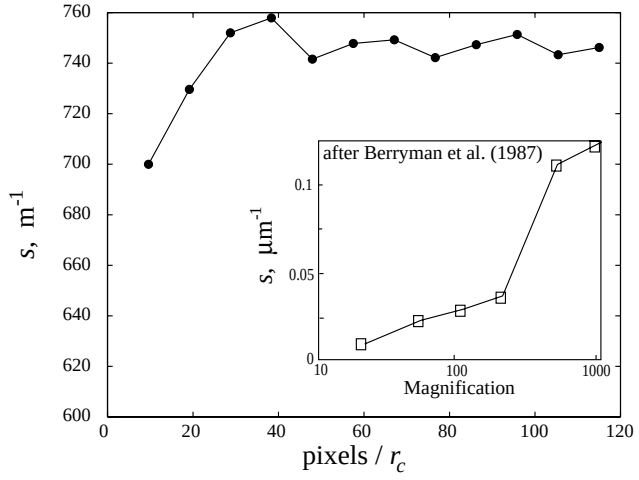

Figure 4. Specific surface area s for a typical (flow1) sample versus pixels per characteristic bubble radius r_c. Inset: s at different magnifications for a granular material (after *Berryman and Blair* [1987]).

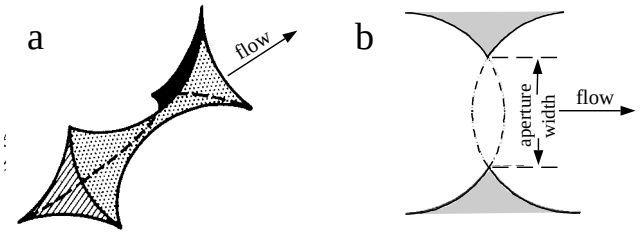

Figure 5. Pathways for a) granular and b) vesicular materials (after *Feng et al.* [1987]).

Image resolution is crucial in determining s because s typically increases with increasing magnification (inset of Fig. 4) [*Berryman and Blair*, 1987]. This effect is problematic in granular material, where the resolution of narrow inter-grain pathways (Fig. 5a) strongly influences s. In contrast, s obtained from pathways formed by overlapping bubbles (Fig. 5b) does not increase above a minimum resolution of about 30 pixels per median bubble radius r_c (Fig. 4). Porosities determined by image analysis and measured ϕ agree to within about 5% (Fig. 6). Thus, cores are represented reasonably well by the scanned images.

Figure 7 shows the divergence of calculated and measured k. In general, k is overestimated by several orders of magnitude for samples containing bubbles. While granular materials are well-represented by the equivalent channel model [e.g., *Blair et al.*, 1996], inter-bubble apertures determine k in vesicular basalt. Determining aperture sizes

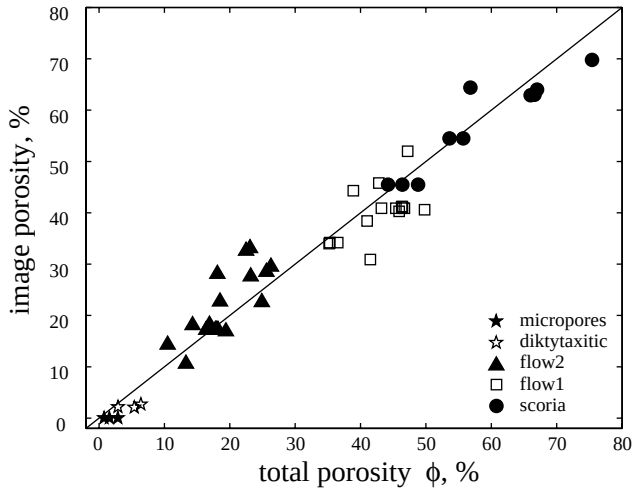

Figure 6. Porosity determined by image analysis versus total porosity.

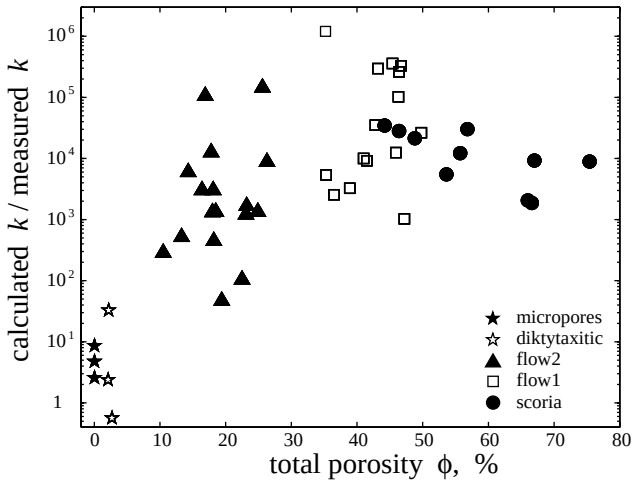

Figure 7. Ratio of calculated to measured permeability k (indicating overestimation of k) versus total porosity ϕ for all samples.

requires resolving the 3D pore structure whereas image analysis resolves bubble cross sections. In contrast, diktytaxitic rocks contain inter-crystalline micropores and thus pathway geometries resembling granular materials. Calculated and measured k of bubble-free, diktytaxitic basalts therefore differ by less than about an order of magnitude.

Although models such as equation (2) cannot successfully calculate k for vesicular rocks, these models do, in fact, provide information about microstructure. In particular, $k \sim l_c^4$ for a fixed number of pathways [equation (6.2.2.4) in *Scheidegger,* 1960], where l_c is the characteristic pore dimension, in this case the aperture radius. Because calculated k is typically $O(10^4)$ larger than measured k, the mean aperture size is $O(10)$ times smaller than the mean bubble size obtained from image analysis.

Acknowledgments. K.V. Cashman is thanked for ideas. D. Senkovich and C. Ambers helped build the permeameter, and L. Chitwood provided some samples. L. Carlson granted a sampling permit. This work was supported by the NSF and the Petroleum Research Fund.

References

Archie, G. E., The electrical resistivity log as an aid in determining some reservoir characteristics, *Trans. Am. Inst. Min. Metall. Pet. Eng., 146,* 54-62, 1942.

Bear, J. *Dynamics of Fluids in Porous Media,* 764 pp., Dover Publications Inc., New York, 1988.

Berryman, J. G., Measurement of spatial correlation functions using image processing techniques, *J. Appl. Phys., 57,* 2374-2384, 1985.

Berryman, J. G., Relationship between specific surface area and spatial correlation functions for anisotropic porous media, *J. Math. Phys., 28,* 244-245, 1987.

Berryman, J. G., and S. C. Blair, Kozeny-Carman relations and image processing methods for estimating Darcy's constant, *J. Appl. Phys., 62,* 2221-2228, 1987.

Blair, S. C., P. A. Berge, and J. G. Berryman, Using two-point correlation functions to characterize microgeometry and estimate permeabilities of sandstones and porous glass, *J. Geophys. Res., 101,* 20,359-20,375, 1996.

Bosl, W. J., J. Dvorkin, and A. Nur, A study of porosity and permeability using a lattice Boltzmann simulation, *Geophys. Res. Lett., 25,* 1475-1478, 1998.

Carman, P. C. *Flow of Gases Through Porous Media,* 182 pp., Academic, San Diego, Calif., 1956.

Cashman, K. V., M. T. Mangan, and S. Newman, Surface degassing and modifications to vesicle size distributions in active basalt flows, *J. Volc. Geotherm. Res., 61,* 45-68, 1994.

Chitwood, L., Inflated basaltic lava; examples of processes and landforms from central and Southeast Oregon, *Oregon Geology, 56,* 11-20, 1994.

Dullien, F. A. L., *Porous Media - Fluid Transport and Pore Structure,* 2nd edition, 574 pp., Academic, San Diego, Calif., 1992.

Feng, S., B. I. Halperin, and P. N. Sen, Transport properties of continuum systems near the percolation threshold, *Phys. Rev. B, 35,* 197-214, 1987.

Freeze, R. A., and J. A. Cherry, *Groundwater,* 604 pp., Prentice-Hall, Englewood Cliffs, 1979.

Ingebritsen, S. E., and M. A. Scholl, The hydrology of Kilauea volcano, *Geothermics, 22,* 255-270, 1993.

Klug, C., and K. V. Cashman, Permeability development in vesiculating magmas: implications for fragmentation, *Bull. Volc. 58,* 87-100, 1996.

Manga, M., A model for discharge in spring-dominated streams and implications for the transmissivity and recharge of quaternary volcanics in the Oregon Cascades, *Water Resour. Res., 33,* 1813-1822, 1997.

Mukhopadhyay S., and M. Sahimi, Scaling behavior of permeability and conductivity anisotropy near the percolation threshold, *J. Stat. Phys., 74,* 1301-1308, 1994.

Paterson, M. S., The equivalent channel model for permeability and resistivity in fluid-saturated rock – A re-appraisal, *Mech. Mater.,* 345-352, 1983.

Saar, M. O., The relationship between permeability, porosity, and microstructure in vesicular basalts, M.S. thesis, 91 pp., University of Oregon, June 1998.

Sahimi, M., *Applications of Percolation Theory,* 258 pp., Taylor and Francis, London, Bristol, PA, 1994.

Sahimi, M., *Flow and Transport in Porous Media and Fractured Rock,* 482 pp., VCH Verlagsgesellschaft mbH, Weinheim, Germany, 1995.

Sanford, W. E., Correcting for diffusion in carbon-14 dating of ground water, *Groundwater, 35,* 357-361, 1997.

Scheidegger, A. E., *The Physics of Flow through Porous Media,* 313 pp., University of Toronto Press, 1960.

Sen, P. N., C. Scala, and M. H. Cohen, A self-similar model for sedimentary rocks with application to the dielectric constant of fused glass beads, *Geophysics, 46,* 781-795, 1981.

M. Manga and M. Saar, Department of Geological Sciences, University of Oregon, Eugene, OR 97403-1272. (e-mail: martin@newberry.uoregon.edu; manga@ newberry.uoregon.edu)

(Received September 8, 1998; revised October 20, 1998; accepted November 24, 1998.)